QIRT 10
http://dx.doi.org/10.21611/qirt.2010.037
10th International Conference on Quantitative InfraRed Thermography
July 27-30, 2010, Québec (Canada)

Evaluation of FRP gluing on concrete structures by active infrared thermography

by J. Dumoulin*, C. Ibarra-Castanedo**, M. Quiertant*, F. Taillade*, A. Bendada** and X. Maldague**

*Université Paris-Est, Laboratoire Central des Ponts et Chaussées (LCPC), 58 Bd Lefebvre, 75732 Paris Cedex 15, France, {jean.dumoulin, marc.quiertant, frederic.taillade}@lcpc.fr
**Computer Vision and Systems Laboratory, Pavillon Adrien-Pouliot, Laval University, Quebec (PQ) Canada, G1V 0V6, {IbarraC, Bendada, MaldagX}@gel.ulaval.ca

Abstract

The strengthening or retrofitting of reinforced concrete structures by externally bonded Fiber Reinforced Polymer systems is now a commonly accepted and widespread technique. Durability of such repairing technique leans by part on the good quality of the gluing of FRP on site. Among the Non-Destructive Evaluation (NDE) techniques under investigation for bonding quality assessment, active infrared thermography is of particular interest given its relatively easiness of deployment and rapidity to inspect large surfaces for which only one side is accessible. In this paper, numerical simulation and experiments were performed and pulse heating and square heating excitations were investigated. A first set of tests with the pulsed phase thermography algorithm were carried out for defect depth retrieval.

1. Introduction

The strengthening or retrofitting of reinforced concrete structures by externally bonded Fiber Reinforced Polymer systems is now a commonly accepted and widespread technique . However, the use of bonding techniques always implies following rigorous installing procedures [1-3]. Moreover installation crews have to be trained in accordance with the installation procedure to ensure the durability and long-term performance of the FRP reinforcements. Conformance checking through an in situ auscultation of the bonded FRP systems is then highly suitable. The quality-control program should involve a set of adequate inspections and tests. Visual inspection and acoustic sounding (hammer tap) are commonly used to detect delaminations (disbonds) but are unable to provide sufficient information about the depth (in case of multilayered composite) and width of debonded areas and are not capable of evaluating the level of adhesion between the FRP and the substrate (partial delamination, damage of the resin, poor mechanical properties of the resin). Consequently, rapid and efficient inspection methods are required. Among the non destructive methods under study, active infrared thermography was investigated due to its ability to be used on field.

Previous works were carried out on such type of reinforcement for one geometry (circular) of defect and nature (polytetrafluoroethylene) [4]. In the present study different types of defaults were inserted, at a same depth, between the concrete substrate and the pultruded CFRP laminate plate glued to its surface. All these defects have different heat capacities and shapes. Experiments were conducted in laboratory on dedicated samples and also by using 3D numerical simulation. The thermal signature for different geometries and nature of defects are studied for pulse and square heating thermal excitation.

2. Experimental set-up and numerical simulations

2.1. Sample characteristics

In parallel samples were reinforced with CFRP plates (provided by SIKA Canada) externally bonded on concrete blocks. Various types of defects (wood, steel, Teflon, cork...) were inserted in the glue layer during fabrication. Fig. 1 shows two photographs of the samples fabricated in laboratory.

http://dx.doi.org/10.21611/qirt.2010.037
10th International Conference on Quantitative InfraRed Thermography

Fig. 1. *Artificial defects on the concrete block before gluing the laminates (left picture); and the two samples with CFRP laminate plates glued on cement concrete blocks (right picture).*

In the present paper, analysis of results obtained for four of the defects shown in Fig. 1 is presented. These defects are a Teflon disk, cork and steel squares of two different extensions but same thickness, and a wood rectangle.

The main characteristics of CFRP plates (Carbodur 1012 provided by SIKA Canada), epoxy resin and cement concrete are reported in Table 1, which also reports the thermal properties taken into account for defects.

Table 1. *Main characteristics and thermal properties of the constitutive elements of the samples.*

Material	**Geometric characteristics**	**k ($W.m^{-1}.K^{-1}$)**	**ρ ($kg.m^{-3}$)**	**Cp ($J.kg^{-1}.K^{-1}$)**
SIKA Carbodur 1012 (CFRP)	460 mm (L) x 100 mm (W) x 1.2 mm (D)	4.2 || fibers 0.7 ⊥ fibers	1530	840
Epoxy resin : Sikadur - 30	460 mm (L) x 170 mm (W) x ~1 mm (D)	0.2	1200	1220
Cement concrete bloc	460 mm (L) x 170 mm (W) x 100 mm (D)	1.8	2300	920
Wood	20 mm (L) x 10 mm (W) x 1 mm (D)	0.15	600	1900
Steel	40 mm (L) x 40 mm (W) x 1 mm (D)	15.1	8055	480
Teflon	20 mm (Diameter) x 1 mm (D)	0.235	2200	1050
Cork	20 mm(L) x 40 mm (W) x 1 mm (D)	0.039	120	1800

2.2. Experimental test bench

Samples were submitted to two types of thermal excitation. The first one was a short pulse heat stimulation using two “BALCAR” flashes of 3,200 J with a duration pulse of 10 ms. The second one was a long square heating pulse of 10, 30 and 60 s using two halogen lamps of 1,000 W each. For both configurations distance between the sample and the lamps was 1 m. Lamps were positioned at a 45° angle for both pulsed and square heating. A schematic representation of the test bench is presented in Fig. 2.

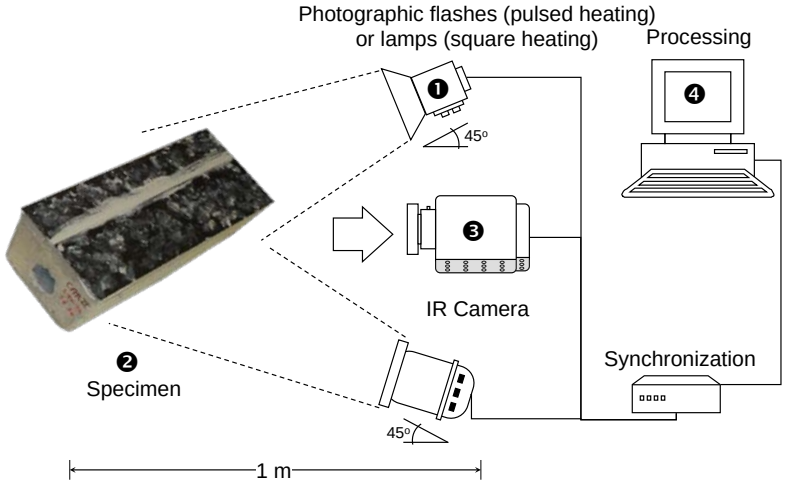

Fig. 2. *Scheme of the laboratory test bench.*

A FLIR MWIR IRFPA camera was used during trials. For pulse excitation thermal image acquisition frequency was set to 22Hz. For square heating excitation 3 acquisition frequencies were used: 11 Hz for 10 s step, 5.5 Hz for 30 s square and 4.4 Hz for 60 s step.

2.3. Numerical simulations

Numerical simulations were accomplished using Finite Element Method (FEM). A 3D model of a cement concrete parallelepiped bloc was realized under COMSOL. Different defects were inserted on the surface of this bloc (see Fig. 3a). The bloc size is the same as the laboratory samples and its depth is of 4 cm, which is sufficiently thick to assume that its rear face would not be affected by the thermal wave generated by the two kinds of thermal stimulation studied herein.

As for the experimental samples, CFRP plates with same characteristics were inserted on top of the concrete block. An epoxy resin layer of 1 mm between the concrete and CFRP plates was considered. A gap of 10 mm compound filled with epoxy resin was left between the two plates.

For the numerical simulation 3 defect geometries were considered: rectangular, square and circular, all with a thickness of 1 mm. An illustration of the geometry and of the mesh is given in Fig. 3b for various defects inserted between CFRP and concrete.

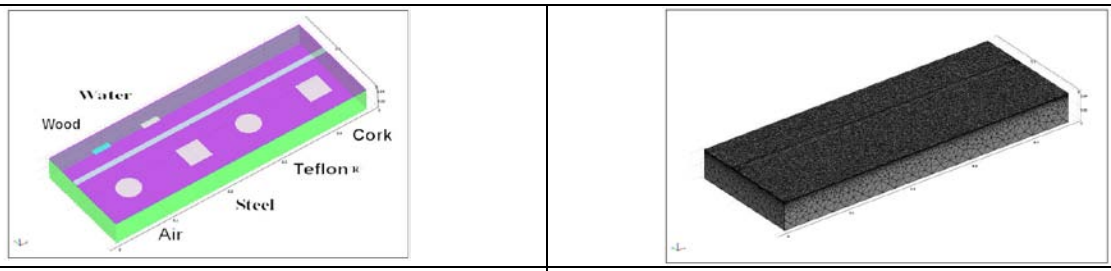

(a) (b)

Fig. 3. *Illustration of numerical simulation: (a) distribution of different defect types, and (b) FE meshing made with COMSOL.*

The influence of the thermal excitation nature (Dirac pulse or square pulse), for different numerical configurations, was studied in terms of time evolution of the defect thermal signature. No additional thermal resistance at the interfaces were considered for numerical simulations. The thermal signatures of the different kinds of defects numerically inserted in the glue layer between the concrete substrate and the FRP composite were also simulated. The 3 defect geometries designed for numerical simulations have the same dimensions independently of their nature. The thickness of all defects was 1 mm, which is the same as the resin epoxy layer. The disk defect has a diameter of 40 mm, the rectangle defect size is 30 mm (L) x 10 mm (W) and the size of the square defect side is 40 mm.

The block was assumed to be insulated on its lateral faces. First type of boundary condition was fixed on concrete block rear surface (temperature was 293.15 K). Front face (CFRP) is submitted to a heat pulse and in a first approach a mean heat transfer coefficient of 10 $W.m^{-2}°C$ was included to the boundary conditions for this face. Thermal properties reported in Table 1 were used for computation.

It should be noticed that for all simulations no contact thermal resistance was considered between upper and lower boundaries of defects.

3. Results and analysis

3.1. Localization of defect using singular value decomposition on experimental data

Singular value decomposition (SVD) is an interesting tool for the extraction of the spatial and temporal information from a thermal image sequence in a compact or simplified manner. The SVD of an *MxN* matrix **A** (*M>N*) can be calculated as follows [5-6]:

$$\mathbf{A} = \mathbf{U}\mathbf{R}\mathbf{V}^T \quad (1)$$

where **U** is an *MxN* orthogonal matrix, **R** being a diagonal *NxN* matrix (with the singular values of **A** in the diagonal) and $\mathbf{V}^T$ is the transpose of an *NxN* orthogonal matrix (characteristic time).

After rearranging the thermal image for every time as columns in **A** and applying the SVD, the columns of U represent a set of orthogonal statistical modes known as empirical orthogonal functions (EOF) that describes spatial variations of data. On the other hand, the principal components (PCs), which represent time variations, are arranged row-

http://dx.doi.org/10.21611/qirt.2010.037
10th International Conference on Quantitative InfraRed Thermography

wise in matrix $\mathbf{V}^T$. The first EOF will represent the most characteristic variability of the data; the second EOF will contain the second most important variability, and so on. Usually, original data can be adequately represented with only a few EOFs [7-8]. SVD computations were performed on experimental thermal images sequences for pulse and square heating acquired at different frequencies. It has to be noticed that for pulse heating only the thermal relaxation is recorded and for the square heating thermal image sequence starts at the beginning of the sample heating.

Fig. 4 shows defect localization obtained on laboratory samples CAR I and CAR II with optical thermal pulse excitation of 10 ms on the raw surface without cleaning (see Fig. 1). Even in this non favourable configuration defects can be detected.

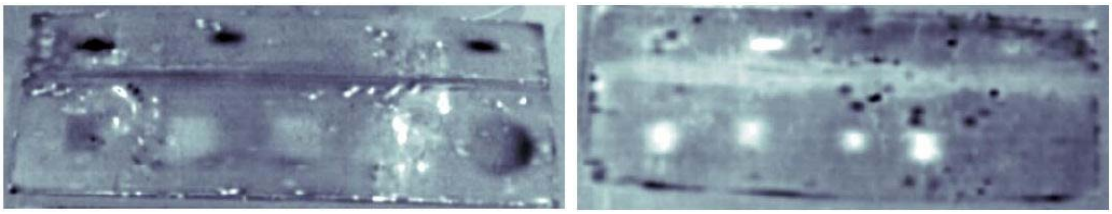

Car I *Car II*

Fig. 4. *Results with principal component analysis on pulsed thermography data obtained from laboratory experiments using the photographic flashes on specimens CAR I (left) and CAR II (right).*

Fig. 5 shows defect localization obtained on laboratory samples CAR I and CAR II with optical square heating excitation of 30 s on the raw surface.

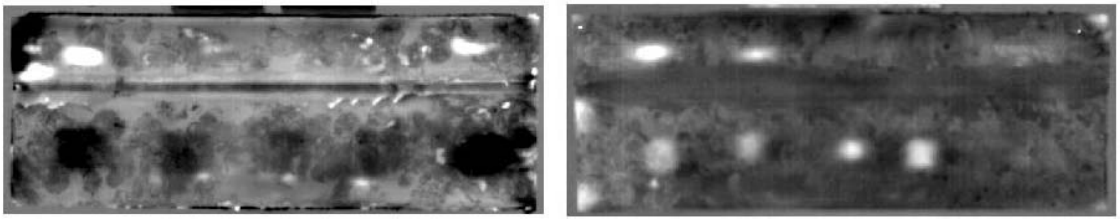

Car I *Car II*

Fig. 5. *Results with principal component analysis on square heating thermography data obtained from laboratory experiments using the photographic flashes on specimens CAR I (left) and CAR II (right).*

In following paragraph, faulty and sound areas used for computation were localised by using these EOF maps.

3.2. Simulated and experimental thermograms

Fig. 6 shows the thermal profiles for defective and non-defective (sound) areas obtained by numerical simulations for 10 ms pulse heating and 30 s square heating. As can be seen from these profiles, cork and wood defects produce a positive thermal contrast with respect to the sound area. On the contrary, steel and Teflon® produce a negative contrast.

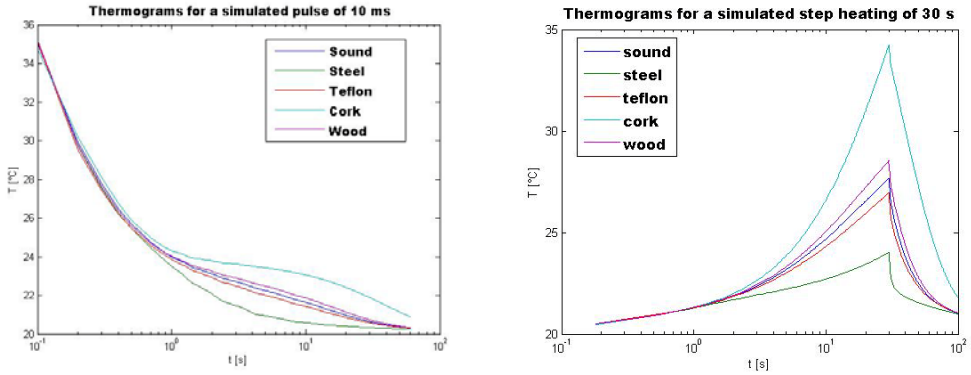

Fig. 6. *Pulse and square heating thermograms extracted from numerical simulations.*

Contrary to simulated data, experimental thermograms were greatly affected by non-uniform heating and emissivity variations due to the presence of glue residues in the surface (see Fig. 1 right and Fig. 2) as can be seen in Fig. 7. The PCT

http://dx.doi.org/10.21611/qirt.2010.037

results (first EOF) presented in Fig. 7 contain indication on the homogeneity of thermal excitation. In particular, to intensive heat area may be observed over CAR I.

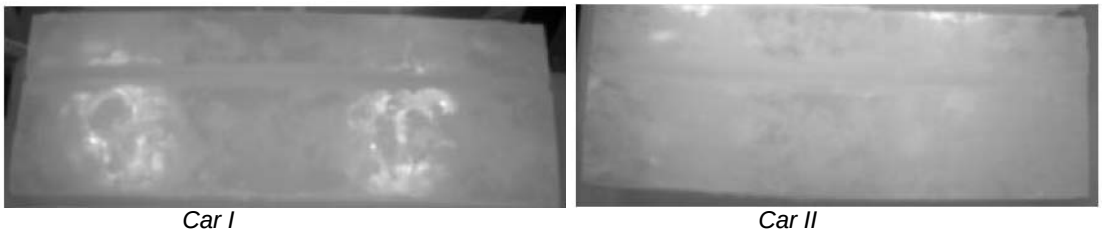

Car I *Car II*

Fig. 7. *First EOF map computed with experimental pulse heating thermal image sequence*

Fig. 8 shows the experimental thermal profiles for both samples, Car I (left) and Car II (right) for the pulsed heating (top) and the square heating (bottom) experiments for the same type of defects considered in the simulations. The specimen Car I contained steel and wood type defects, whilst specimen Car II contained cork and Teflon® type defects. Sound areas next to these defects were selected in order to minimize the effect of non-uniformities.

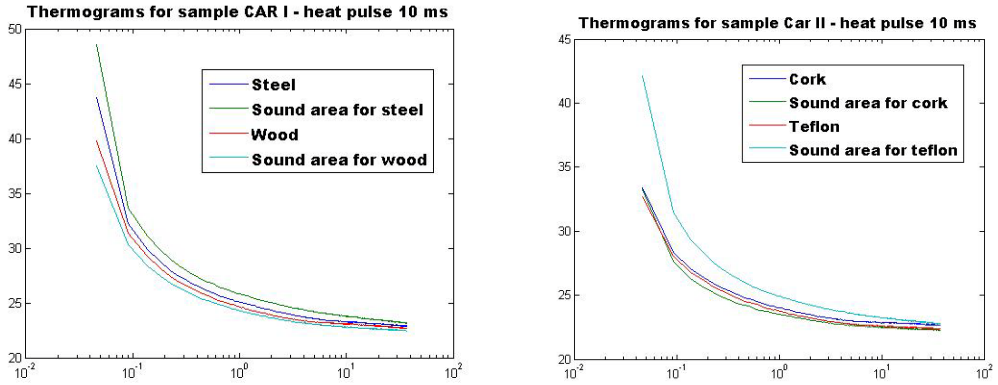

Pulse heating

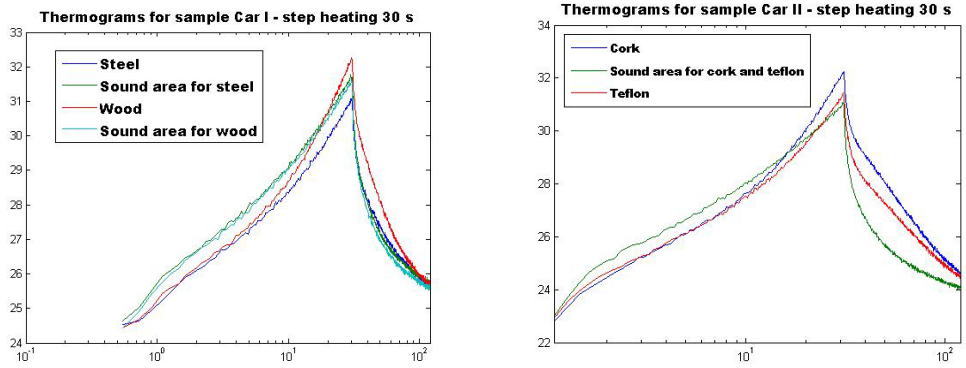

Square heating of 30 s

Fig. 8. *Pulse and square heating thermograms extracted from experimental thermal image sequences*

In the case of pulsed heating excitation (Fig. 8, top), the thermal profiles for all types of defects qualitatively follow the same behaviour predicted by the simulation (Fig. 6 left), i.e. the less effusive materials (cork and wood, see Table 2) produce a positive contrast and the more effusive (steel and Teflon®, see Table 2) a negative contrast with respect to the sound areas (individually selected next to the defective areas to minimize non-uniformities). In the case of square heating however, the situation is different for the case of more effusive materials. For instance, the thermal profile for steel (Fig. 8, bottom-left) follows the behaviour predicted by simulation during heating but this trend is inverted during the cooling stage. This is probably due to the presence of a thermal resistance in the interface between the steel and the epoxy. Furthermore, the actual size of this defect is less than the one considered for numerical simulations. In addition, the epoxy layer is probably

more than 1 mm thickness due to fabrication conditions in laboratory (i.e. training professional generally succeed in having a finished thickness between 0.5 to 1 mm).

For the Teflon® defect, a similar behaviour can be noticed, although in this case, the trend is inverted before the heating stage has finished and continues during the cooling stage. For such defect in Teflon® it is expected to have a positive contrast versus sound area when only its thermal resistance is considered and presence of lateral epoxy resin is neglected, in particular if it has a negligible volume, hypothesis commonly adopted for 1D geometries for flaw in composites. Nevertheless, in this 3D approach, defect is inserted in an epoxy layer of a non-negligible thickness, so thermal effusivity of epoxy resin and CFRP versus Teflon needs to be considered. Table 2 reports the main thermal characteristics of the studied material (thermal resistances and effusivities).

Table 2. Thermal resistance and effusivity for the materials.

Material	Thermal resitivity (see table 1 for depth) in [W.°C^{-1}]	Thermal effusivity in [W.s$^{1/2}$.m^{-2}.K^{-1}]	Effusivity ratio: CFRP/Material type	Effusivity Ratio: Epoxy resin/Material type
CFRP	0.0017	948.5	1.00	0.57
Epoxy	0.0050	542.5	1.75	1.00
Air	0.0413	5.5	173.65	99.31
Water	0.0017	1582.6	0.60	0.34
Wood	0.0067	413.5	2.29	1.31
Teflon	0.0043	736.8	1.29	0.74
Cork	0.0256	91.8	10.33	5.91
Steel	6.62E-05	7640.9	0.12	0.07

From Table 2 it is noticed that Teflon is the only material considered herein for which the effusivity ratio with respect to CFRP is higher than 1 ($e_{cfrp/Teflon}$=1.3) and the effusivity ratio with respect to epoxy resin is lower than 1 ($e_{epoxy/Teflon}$=0.7). This could explain the differences between 3D simulated analysis and the experimental results

These experimental and simulated thermal profiles are next used to calculate the defects thermal contrast evolution.

3.3. Contrast evolution with time

As defective and sound areas were previously localized using SVD image processing for experimental data and known for numerical simulations, the running contrast [9] was chosen in order to reduce the impact of non-uniformity of heating and to analyse the thermal signature of each defect time versus time evolution for pulse and square heating excitations. Its formulation is recalled in equation 2.

$$\Delta T(t) = \frac{T_d(t) - T_{S_a}(t)}{T_{S_a}(t)} \qquad (2)$$

Fig. 9 shows the running contrast results calculated with simulated data for a 10 ms pulse heating and a 30 s square heating.

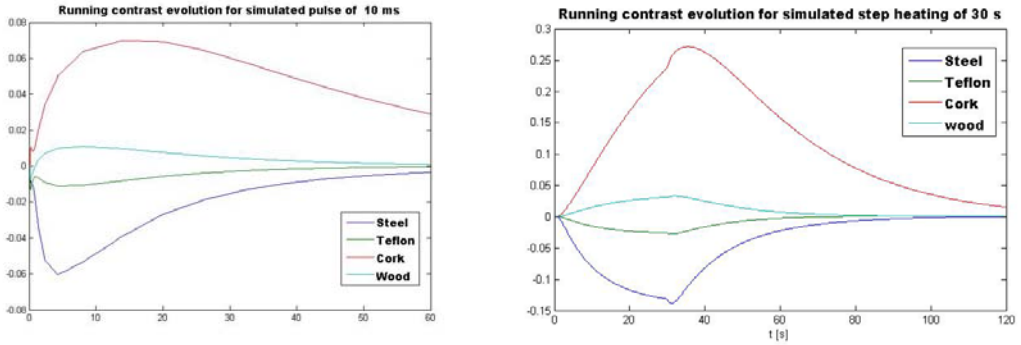

Fig. 9. *Pulsed and square heating running contrast evolution calculated with numerical simulations*

Fig. 10 shows running contrast computed using experimental thermograms presented in the previous paragraph.

http://dx.doi.org/10.21611/qirt.2010.037

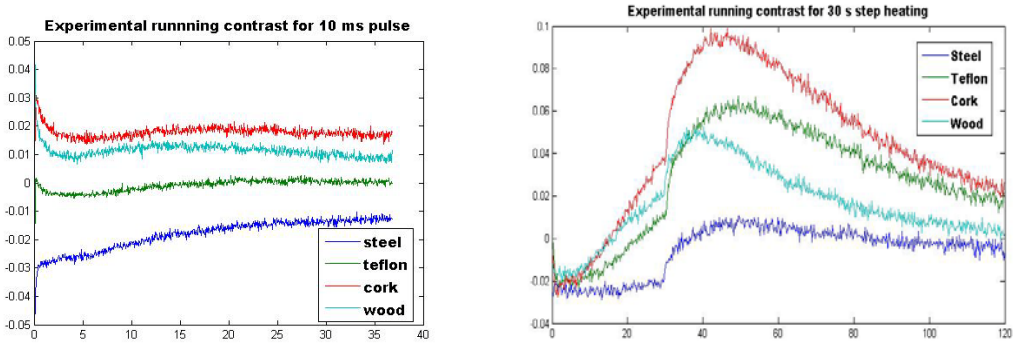

Fig. 10. *Pulsed and square heating running contrast evolution calculated with experimental data*

Results from these two graphs confirmed the observations made from Fig. 6 and Fig. 8, i.e. the experimental profiles follows the tendency predicted by the simulation for all defect types for the case of pulsed heating, but only partially for the case of square heating.

It is also noted that thermal contrast is very weak for the pulsed experiment. The surface condition (presence of glue residues) could contribute to reduce the thermal signature of defects. A second set of experiments with a clean surface could more closely reproduce the simulated profiles. For the case of square heating, thermal contrast is higher since more energy is delivered to the surface. These thermal contrasts could be used to estimate the depth defect using the procedure presented in ref [13].

3.4. Depth estimation with the phase

Pulsed phase thermography (PPT) [10] is another interesting technique, in which data is transformed from the time domain to the frequency domain using the one-dimensional discrete Fourier transform (DFT). The phase is of particular interest in NDE given that it is less affected than raw thermal data by environmental reflections, emissivity variations, non-uniform heating, and surface geometry and orientation.One of the most interesting characteristics of the phase is the possibility of performing straightforward quantitative operations. A direct relationship exists between the depth of a defect and the thermal diffusion length, μ, which can be exploited through a relationship of the form [11]:

$$z = C_1 \cdot \mu = C_1 \sqrt{\frac{\alpha}{\pi \cdot f_b}} \tag{3}$$

where C_1 is an empirical constant that has been estimated to be 1.8, and f_b [Hz] is the blind frequency [11].

In Fig. 11, the thermal and phase profiles for a defect (steel on specimen Car I) are presented. These graphs show the profiles for raw and synthetic data. Synthetic data was reconstructed from a 4th degree polynomial regression, following the procedure described by Shepard [12]. This allowed to determine the blind frequency required to estimate the depth through Eq.(3).

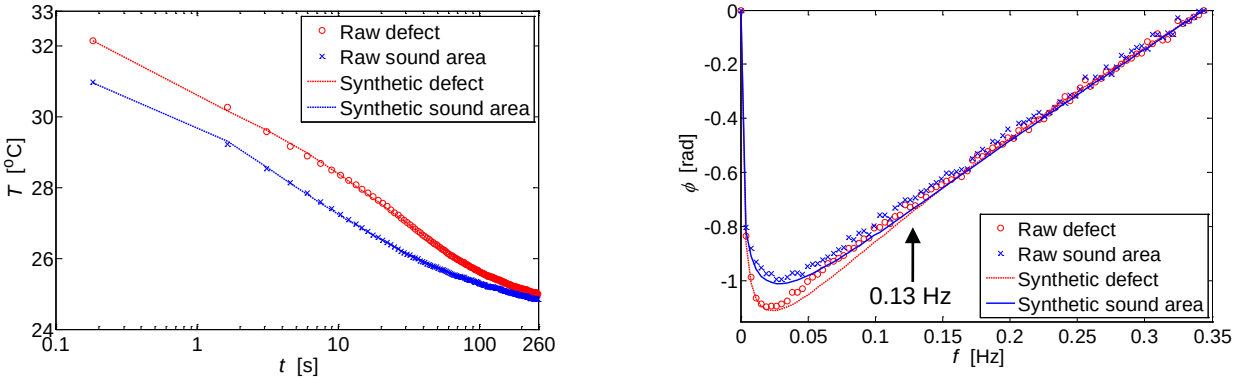

Fig. 11. *Raw and synthetic (a) thermal profiles; and (b) PPT profiles, for a defective (steel) and non-defective areas.*

Introducing the thermal properties of CFRP reported in Table 1 in Eq.(3), the depth of this defect is estimated to be z=2.01 mm, which is close to the value reported in Table 1. However, this depth was estimated using exclusively the thermal properties of CFRP. The material beneath defects is in fact a bi-layer structure (neglecting air at the interfaces) composed by CFRP (z=1.2 mm, see Table 1) and an epoxy layer (z~1 mm, see Table 1). Hence, thermal properties of this bi-layer structure are a combination of the thermal properties of the two materials. If we hypothetically consider that the material beneath the defect is constituted by a mono-layer of epoxy material, depth estimation results on z=1.02 mm. The depth of the steel depth can thus be roughly situated between 1 and 2 mm.

4. Conclusion

Numerical 3D simulations were combined with experiments on laboratory samples to study the thermal signature of artificial defects inserted between a CFRP plate and a cement concrete bloc. Two kinds of optical thermal excitation were investigated: pulse and square heating. As such CFRP plates are used to reinforce civil engineering structure, active infrared thermography is one of the techniques presently considered to control the gluing phase in situ. Hence, in order to complete the qualitative analysis, which drives to defect detection, thermal excitation has to be further investigated in terms of maneuverability on site and its adequacy for quantitative analysis. Laboratory studies and numerical simulations are valuable tools to define typical trials on real site. For instance, a depth estimation example using experimental and synthetic data from a steel defect was presented. The depth estimation results are affected by the phase noise, synthetic data allowed to better estimate the blind frequency required in the process. However, Eq.(3) used for the computations is only valid for mono-layer materials. The case in hand is in fact a bi-layer structure (neglecting air in the interfaces). The thickness of the epoxy layer is only an estimate and might contribute to the incertitude on the result.

Acknowledgements:

Authors wish to thank Richard Sherping from SIKA Canada Inc for providing CFRP plates and epoxy glue and to the Canada Research Program (CRC): Multipolar Infrared Vision Canada Research Chair (MiViM) for supporting part of this research**.** Part of this work also received funding from the European Community's Seventh Framework Program (FP7/2007-2013) under Grant Agreement n° 225663 Joint Call FP7-ICT-SEC-2007-1 **(ISTIMES project:** *Integrated System for Transport Infrastructures surveillance and Monitoring by Electromagnetic Sensing*)***.***

REFERENCES

[1] ACI Committee 440.2R02-08."Guide for the Design and Construction of Externally Bonded Systems for Strengthening Concrete Structures", American Concrete Institute, Michigan, U.S.A., 2008.
[2] AFGC. (2007). "Réparation et renforcement des structures en béton au moyen des matériaux composites – Recommandations provisoires", Bulletin scientifique et technique de l'AFGC. (in French).
[3] Fib Task Group 9.3. (2001) Externally bonded FRP reinforcement for RC structures, fib bulletin 14, Lausanne, Switzerland.
[4] F. Taillade, J. Dumoulin, M. Quiertant, C. Ibarra-Castanedo, Ch. Aubagnac, X. Maldague and A. Bendada, " Active Infrared Thermography and Shearography applied to non destructive testing of bonded FRP strengthening systems on concrete structures", AITA 2009 (10th International Workshop on Advanced Infrared Thermography and Applications), Firenze, Italy, 8-11 september 2009.
[5] Rajic N., "Principal component thermography for flaw contrast enhancement and flaw depth characterization in composite structures", Composite Structures, vol 58, pp 521–528, 2002.
[6] Marinetti S., Grinzato E., Bison P. G., Bozzi E., Chimenti M., Pieri G. And Salvetti O. "Statistical analysis of IR thermographic sequences by PCA," Infrared Physics & Technology vol 46 pp 85–91, 2004.
[7] Ibarra-Castanedo C., Gonzalez D. A., Galmiche F., Bendada A. And Maldague X. P., "Recent Research Developments in Applied Physics On signal transforms applied to pulsed thermography" Recent Research Developments in Applied Physics, vol 9, pp 101-127, 2006.
[8] Dumoulin J., Ibos L., Ibarra-Castanedo C., Mazioud A, Marchetti M., Maldague X. and Bendada A., "Active infrared thermography applied to non emergent defects detection on asphaltic pavement samples: experiments and numerical simulations", Proceedings of 10th international workshop on advanced infrared technology and applications (AITA'09), Florence (Italy), 8-11 september 2009.
[9] Maldague, X.P.V., "Theory and practice of infrared technology for non-destructive testing", John Wiley & sons Inc (2001).
[10] Maldague X. P. and Marinetti S. "Pulse Phase Infrared Thermography," *J. Appl. Phys.*, **79**(5):2694-2698, 1996.
[11] Ibarra-Castanedo C. and Maldague X. "Pulsed Phase Thermography Reviewed," *QIRT J.*, **1**(1):47-70, 2004.

[12] Shepard S. M. “Advances in Pulsed Thermography”, *Proc. SPIE - The International Society for Optical Engineering, Thermosense XXVIII*, Orlando, FL, 2001, Eds. A. E. Rozlosnik and R. B. Dinwiddie, **4360**:511-515, 2001.
[13] Taillade, F. ; Quiertant, M. ; Benzarti, K. ; Aubagnac, C. Shearography and Pulsed Stimulated Infrared Thermography applied to a Nondestructive Evaluation of bonded FRP strengthening systems on concrete structures. Construction and Building Materials, 2010, DOI: 10.1016/j.conbuildmat.2010.02.019.